Organic Chloride Salt Interfacial Modified Crystallization for Efficient Antimony Selenosulfide Solar Cells

Muhammad Azam, Yan-Di Luo, Rong Tang, Shuo Chen, Zhuang-Hao Zheng, Zheng-Hua Su, Ali Hassan, Ping Fan, Hong-Li Ma, Tao Chen, et al.

Organic Chloride Salt Interfacial Modified Crystallization for Efficient Antimony Selenosulfide Solar Cells

Muhammad Azam,[a, b] Yan-Di Luo [a, c] Rong Tang,[a] Shuo Chen,[a] Zhuang-Hao Zheng,[a] Zheng-Hua Su,[a] Ali Hassan,[a] Ping Fan,[a] Hong-Li Ma,[c] Tao Chen,[d] Guang-Xing Liang*[a], Xiang-Hua Zhang[c]

[a] Shenzhen Key Laboratory of Advanced Thin Films and Applications, Key Laboratory of Optoelectronic Devices and Systems, College of Physics and Optoelectronic Engineering, Shenzhen University, Shenzhen, 518060, P. R. China

[b] Department of Physics, Faculty of Sciences, University of Central Punjab, Lahore, 54000, Pakistan

[c] Univ Rennes, CNRS, ISCR (Institut des Sciences Chimiques de Rennes) UMR 6226, Rennes, F-35000, France

[d] Hefei National Laboratory for Physical Sciences at Microscale, CAS Key Laboratory of Materials for Energy Conversion, Department of Materials Science and Engineering, School of Chemistry and Materials Science, University of Science and Technology of China, Hefei, Anhui 230026, P. R. China

Abstract

Antimony selenosulfide, $Sb_2(SSe)_3$ is recognized as an excellent photoactive material owing to its light harvesting capability. There is still quit a room to improve the film quality for device performance improvement. Herein, an organic chloride salt (Diethylamine hydrochloride, DEA(Cl)) has been introduced into fabricating $Sb_2(SSe)_3$ solar cells for the first time. A champion of 9.17% PCE (power-conversion-efficiency) has been achieved with relatively improved fill factor (FF) and open-circuit voltage (V_{OC}). It has been revealed that DEA(Cl) successfully interact with $Sb_2(SSe)_3$, which can facilitate the crystallization process to give rise to the closely packed bigger grain sizes and with reduced surface cracks, successfully suppressed the oxidized Sb species (Sb_2O_3) in the $Sb_2(SSe)_3$ film give rise to phase purity, thus directing to superior surface morphology and electrical characteristics of DEA(Cl)-modified $Sb_2(SSe)_3$ absorber films. Chloride modification is thus efficiently helpful for suppressing interfacial defects, improving junction quality and optimized energy level alignment. This facile interfacial modification demonstrates the remarkable potential for efficient $Sb_2(SSe)_3$ solar cells.

Keywords: $Sb_2(SSe)_3$; hydrothermal; crystallization; trap states; interfacial modification

1. Introduction

Metal chalcogenides are considered to be efficient light harvesting materials for photovoltaic applications. Specifically, two types of chalcogenide solar cells, such as, CdTe and $Cu_2(InGa)Se_2$ have crossed PCE over 22%, with exceptional stability under operational conditions.[1] Such efficient results with these thin-film solar cell technologies have triggered excessive motivation in finding novel metal chalcogenide photoactive layers, with special attraction in those comprised of non-toxic and earth-abundant components. Several other semiconducting photo-harvesting materials, such as, $Sb_2(S+Se)_3$ (S = 0 or Se = 0 or different ratio of Se/S), $AgBiS_2$, SnS, and GeSe have been explored for photovoltaic.[2-5] Among these materials, $Sb_2(SSe)_3$ is considered to be efficient photoactive thin-film owing to its excellent opto-electronic characteristics such as an incredible absorption coefficient ($>10^5$ cm^{-1})[6], one-dimensional (1D) crystal structure, and easily tunable bandgap (1.1 to 1.7 eV) by varying S to Se atomic ratio.[7-9] Interestingly, the 1D crystal structure gives an extraordinary favorable circumstance to handle with one of the extensive recombination damages in state-of-art thin-film photovoltaic.[10] According to the Shockley–Queisser limit, the theoretical performance of $Sb_2(SSe)_3$-based devices is estimated to be 32%.[11]

Since the sulfur and selenium have similar ionic radius due to which it can be alloyed with a sequential ratio to form $Sb_2(SSe)_3$ having an identical structure of Sb_2S_3 and Sb_2Se_3.[12-15] Therefore, for the fabrication of $Sb_2(SSe)_3$ thin film, both the vapor and solution-based techniques have been adopted.[16-17] In solution-processed technique (one-step spin-coating deposition), the precursor materials based on Sb, S and Se are dissolved in specific organic solvent to form the $Sb_2(SSe)_3$ thin film.[18-19] Since the absorber films should have high crystallinity and uniformly distributed compact grains morphology, which leads to the favorable electrical transport characteristics. But the one step spin coated method produced films with poor crystallinity and a large number of pinholes in the film, resulting to the increment in charge transfer resistance and carrier's recombination at the interfaces.[20] The two

step deposition technique based on the postselenization of Sb_2S_3 films, is somehow produced $Sb_2(SSe)_3$ thin films with comparatively better crystallinity and uniform surface morphology.[21-22] The device performance based on $Sb_2(SSe)_3$ fabricated through this method has been efficiently improved to ≈8%. On the other hand, the devices based on $Sb_2(SSe)_3$ fabricated through vapor deposition were presented efficiencies from 6 to 9%.[4, 23] Although, for obtaining high crystalline films via vapor deposition method, usually required high annealing temperature, which responsible for the origination of defects due to disintegration of $Sb_2(SSe)_3$ compound into its intermediate components (Se_n, S_n, and Sb_xS_y).[24-25] Most recently, researchers have demonstrated that the hydrothermal process was an effective approach to deposit highly crystalline and uniform $Sb_2(SSe)_3$ films. An improved performance of above 10% was realized for the device fabricated through hydrothermal-synthesized $Sb_2(SSe)_3$ thin film.[7] Therefore, in this research we have employed hydrothermal method for the deposition of $Sb_2(SSe)_3$. In addition to develop highly crystalline absorber layer, the interfacial modification is essential for the quick extraction of photogenerated charge carriers by the charge transfer layers, for efficient device performance. Recently, various researchers have used interfacial engineering to modify the absorber layer via different electron/hole-rich materials, such as, Zn (O, S)/CdS, SnO_x/ZnO, CdS/SnO_2, CuSCN, PbS, V_2O_5.[20, 26-29] Therefore, it is crucial to modify the $Sb_2(SSe)_3$ film surface to improve the carrier's capture efficiency and reduce the carrier's recombination loss at the front and back contacts.

In this study, we present an interfacial modification of $Sb_2(SSe)_3$ film, fabricated through hydrothermal deposition approach by using organic salt DEA(Cl). The corresponding treatment results in uniform morphology with enhanced grain size and crystallinity, suppress the formation of impurity phase Sb_2O_3, reduced defects density, and suitable energy level matching. The optimized DEA(Cl)-treated $Sb_2(SSe)_3$ film effectively improved the performance of the solar cell from 7.41% to 9.17%. Attentive device electrical measurements indicated that the

well-energy level matching results in much favorable junction quality, larger recombination resistance, enhanced built-in potential (V_{bi}), and accordingly improved device parameters.

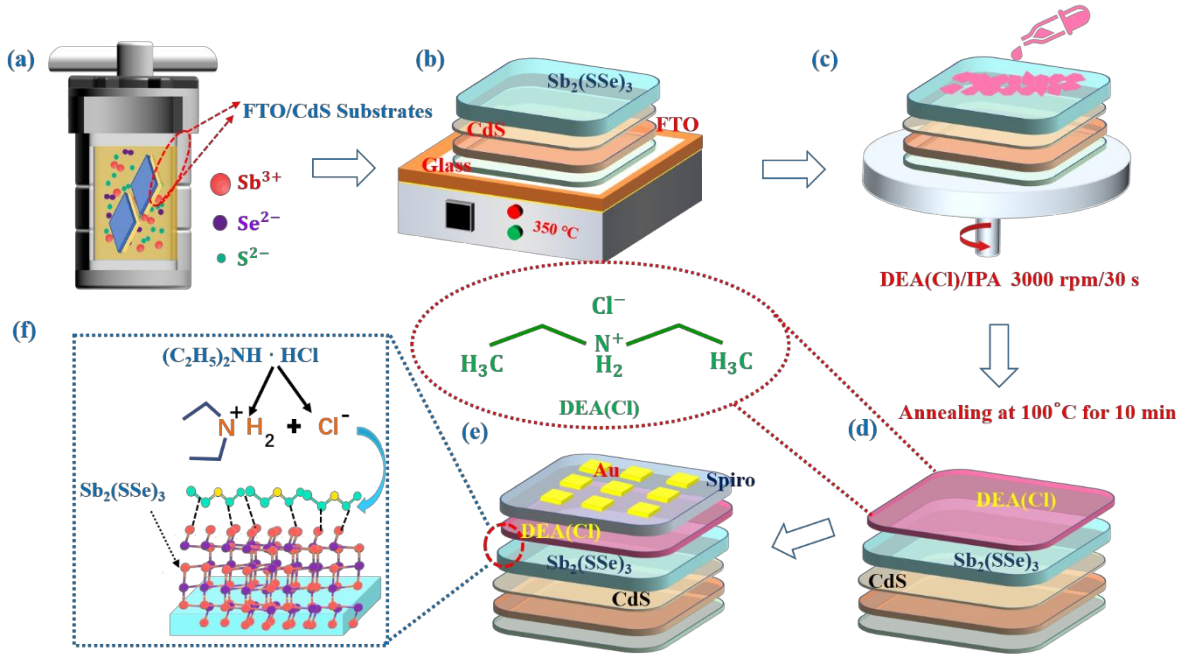

Figure 1. Schematic diagram of $Sb_2(SSe)_3$ solar cell fabrication process, Preparation of $Sb_2(SSe)_3$ by hydrothermal method (a), Annealing $Sb_2(SSe)_3$ film at 350 °C (b), Spin-coating (c) and annealing (d) of DEA(Cl)/IPA solution, Final device structure (e).

2. Results and discussions

The schematic indication of fabricating control and DEA(Cl)-treated $Sb_2(SSe)_3$ thin films is given in Figure 1. For the $Sb_2(SSe)_3$ thin film deposition, we have adopted hydrothermal method, in which the starting precursor materials ($C_4H_4KO_7Sb{\cdot}0.5H_2O$, $Na_2S_2O_3{\cdot}5H_2O$, and CH_4N_2Se) employed as antimony, sulfur, and selenium sources (the detailed procedure is given in the experimental section). The FTO glasses coated with CdS, which is utilized as an electron transport layer fabricated via chemical bath deposition (CBD), were immersed into the autoclave tilted with CdS side facing down (Figure 1a). The corresponding hydrothermal deposition was carried out at an optimized temperature of 140°C for 2 h and 20 min, and then

the samples were transferred to the N_2-glove box for annealing at 350°C (Figure 1b). For the preparation of DEA(Cl)-modified $Sb_2(SSe)_3$ films, the dissolved DEA(Cl)/isopropyl alcohol (IPA) solution was spin-coated on the prepared $Sb_2(SSe)_3$ films, proceeding by annealing at 100°C for 10 min (Figure 1c, d). The whole process of modification of $Sb_2(SSe)_3$ films was accomplished under N_2 filed glove box. The spin-coated DEA(Cl)/IPA solution is supposed to accelerate the diffusion of Cl element to improve the crystallinity of the absorber layer and passivate grain boundaries (Figure 1e), which is beneficial for the V_{OC} and FF enhancement as well as the PCEs.[30] To explore the influence of DEA(Cl) on the crystallinity of the $Sb_2(SSe)_3$ film, we conducted X-ray diffraction (XRD) analysis of the as-fabricated $Sb_2(SSe)_3$ films (Figure 2a). All the respective diffraction peaks are originated between the typical stibnite (orthorhombic) Sb_2Se_3 (PDF#15-0861) and Sb_2S_3 (PDF#42-1393), indicating the production of mixed sulfur and selenium antimony chalcogenide, i.e., $Sb_2(SSe)_3$. It can be observed that the peak intensities are much higher for the DEA(Cl)-modified film compared to the control one, suggesting that the corresponding modification of $Sb_2(SSe)_3$ is remarkably helpful for the crystallization process. Basically, the Cl^- anion in DEA(Cl) organic-halide compound is representative for the advancement in crystallization process, because the Cl^- anion interacts with the S or Se anions partially replaced the corresponding anion, which is proved by our X-ray photoelectron spectroscopy (XPS) results (Figure S1). The interaction of Cl^- with S^- or Se^- is due the resemblance in their ionic radii (176, 179 and 180 Pm, respectively)[31]. Furthermore, there is no apparent expanding of the peak which shows the as-formed $Sb_2(SSe)_3$ demonstrating homogeneous element distribution, instead of gradient chemical impurities.[32] Additionally, we have calculated the crystallite size, the average size for control and modified films were abtained to be 43.70 and 50.80 nm, respectively (Figure S2).

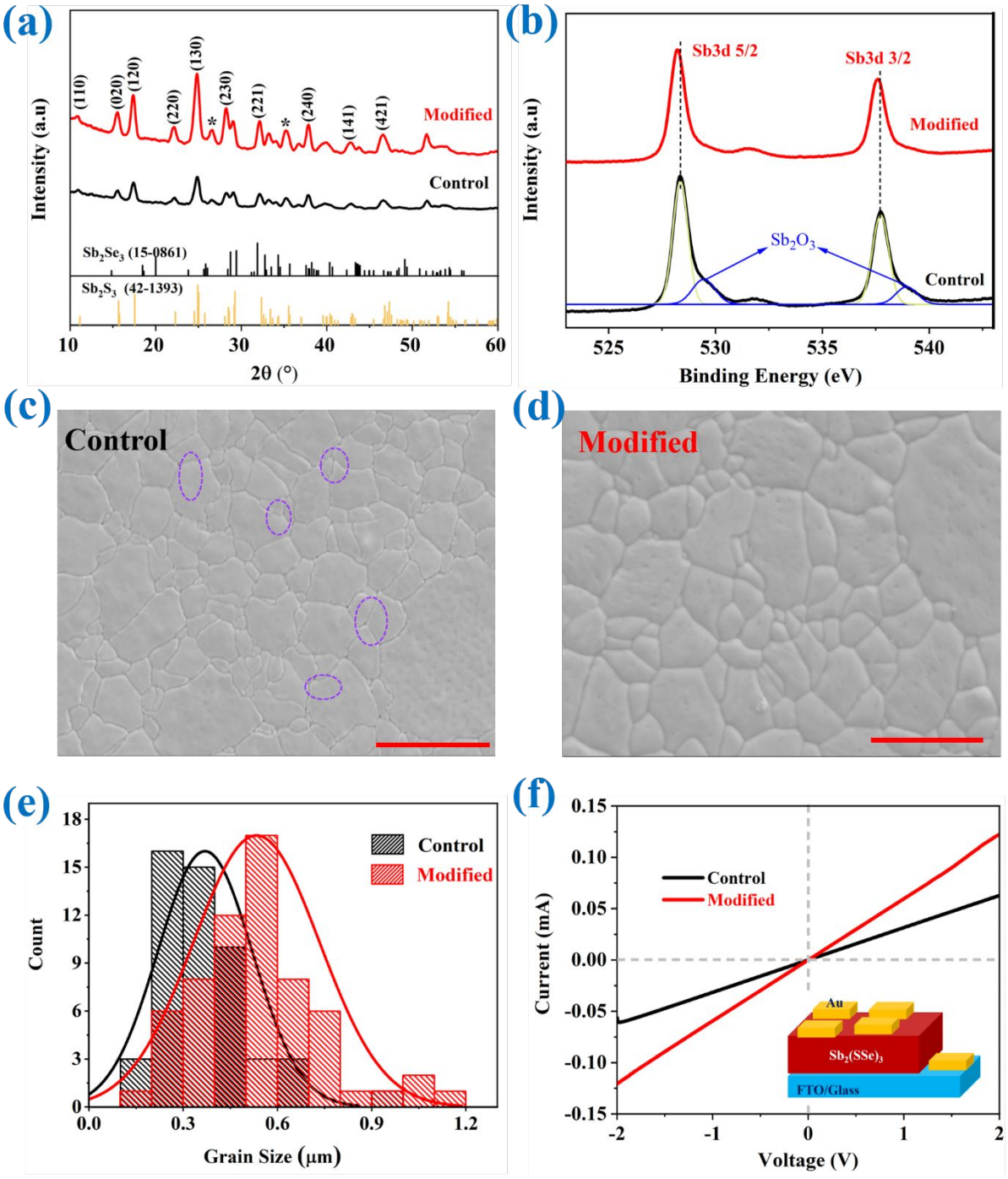

Figure 2. (a) XRD spectra of $Sb_2(SSe)_3$ films with and without DEA(Cl)-treatment spin-coated on the CdS films. (b) Sb 3d XPS patterns of control and modified $Sb_2(SSe)_3$ films. Planer SEM images of (c) control and (d) modified films (Scale bar is 1μm). (e) Statistical analysis of the grain size distribution of $Sb_2(SSe)_3$ films with and without DEA(Cl)-treatment. (f) I–V characteristics of $Sb_2(SSe)_3$ devices based on control and modified films (inset: device structure diagram).

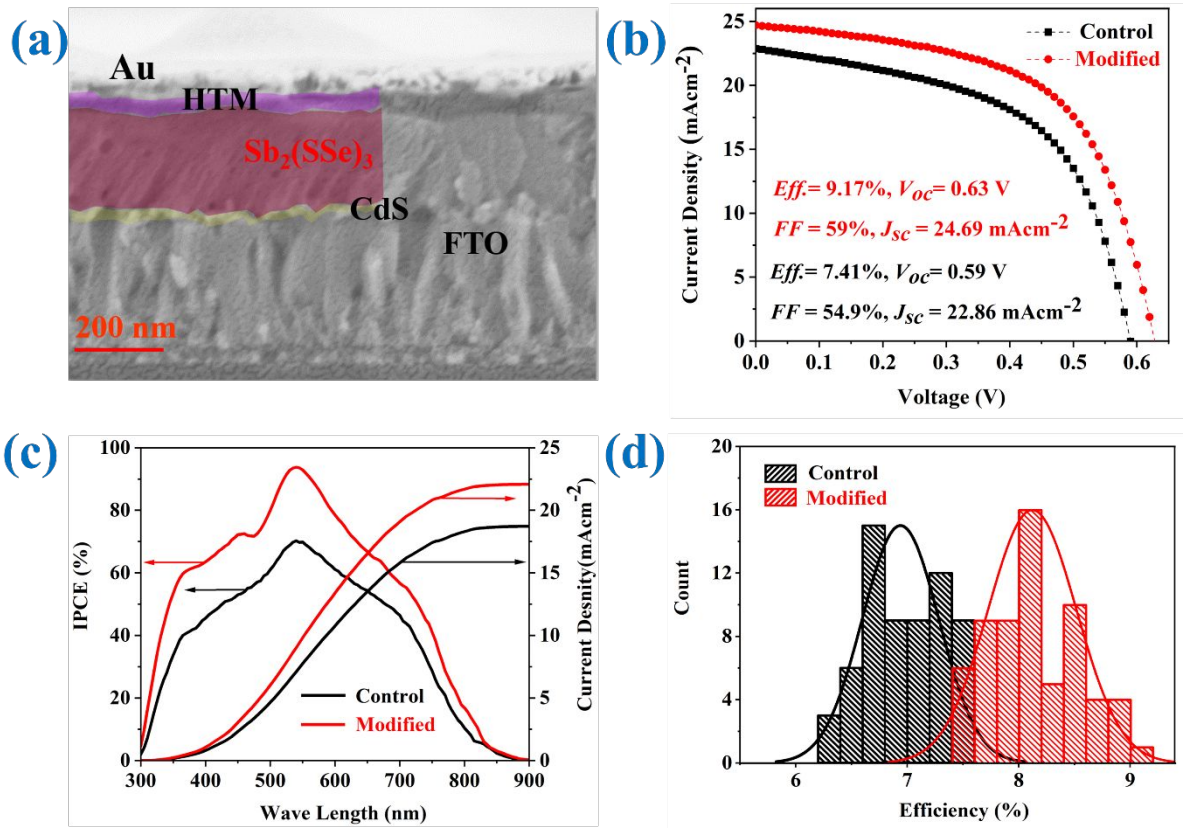

Figure 3. (a) Cross-sectional SEM micrograph of the whole device structure. (b) J–V characteristics, (c) EQE and integrated J_{SC} of the champions devices based on pure and DEA(Cl)-treatment, respectively. (d) A PCE distribution for control and modified devices.

This elemental distribution is also proved by cross-sectional energy-dispersive spectroscopy (EDS) analysis where Sb, S, and Se are uniformly dispersed all over the film (Figure S3, Supporting Information). To clarify the interaction of DEA(Cl) with the $Sb_2(SSe)_3$ surface, we employed XPS and check the high-resolution core-level spectra obtained at varies positions from the sub-surface to the bottom of $Sb_2(SSe)_3$. For the control film, the binding energies of 528.3 and 537.7 eV are related to Sb 3d5/2 and Sb 3d3/2 of $Sb_2(SSe)_3$, respectively, whereas, the peaks at energies 529.1 and 538.9 eV can be attributed to Sb 3d5/2 and Sb 3d3/2 of Sb_2O_3, respectively (Figure 2b).[7] These oxidized peaks are related to the contaminations in the film, which probably originated from the fabrication process or longer period of oxidation under inert environment.[33] On the other hand, the Sb_2O_3 is successfully suppressed in the DEA(Cl)-

modified film, suggesting that there is no oxidized Sb impurity in the $Sb_2(SSe)_3$ active layer, approving the necessarily improved phase purity as confirmed by our XRD results. Additionally, it can be observed that the films with the DEA(Cl)-modification represented an apparent Sb 3d peaks shifting towards the lower binding energy as compared to the control $Sb_2(SSe)_3$, suggesting the charge carrier densities are efficiently enhanced,[34] which could be assigned to the interlinkage with the corresponding organic salt. Through the observations of enhanced crystallization and suppressed impurity phase of $Sb_2(SSe)_3$/DEA(Cl) films, which are proved by our XRD and XPS results, the fast charge transfer and reduced non-radiative recombination at the interfaces for DEA(Cl) modified devices and improved device efficiency is anticipated. Moreover, the Cl 2p spectra of the DEA(Cl)-modified film indicates a clear peak at 196.9 eV, as given in Figure S1, showing that DEA(Cl) is successfully interacted with the $Sb_2(SSe)_3$ film. The high-resolution XPS spectra of S2p, Se3d, and overall spectra are given in Figure S1b, c, and d, respectively, in supporting information. To further study the impact DEA(Cl) on the $Sb_2(SSe)_3$ films morphology, we have carried out scanning electron microscopy (SEM) of control and modified films, as presented in Figure 2c, d. For the control film, a non-uniform morphology is observed with small grain size, apparent pinholes and cracks subsisting in the surface of the film which are highlighted with purple circles (magnified images are given in Figure S4). This poor morphology is destructive for the device performance and stability as the cracks can lead to the shunt paths in the solar cell.[35] On the other hand, the $Sb_2(SSe)_3$ film treated with DEA(Cl) remarkably improve the surface morphology, resulting highly closed packed compact surface and uniformly coverage with enlarge grain size. Moreover, the grain size distribution for the control and modified $Sb_2(SSe)_3$ films is represented in Figure 2e. For the control and modified films, the average grain sizes were calculated to be 369 and 534 nm, respectively. The respective variation in micromorphology represented that optimized interfacial treatment by DEA(Cl) can lead to the improved crystallization and effectively passivate the surface pinholes, which confirms our assumption that the introduction of DEA(Cl)

can reduce nucleation, enhance crystal growth and successfully promote the charge transport leading to the improved device performance.[30, 36] Figure 2f, indicated the dark I-V curves of $Sb_2(SSe)_3$ film modified with and without DEA(Cl). It can be observed that the DEA(Cl) has positive impact on the conductivity of $Sb_2(SSe)_3$ than the pristine one, which demonstrated fast carries transport in DEA(Cl) treated films. The $Sb_2(SSe)_3$ films annealed at 350 °C with and without DEA(Cl) treatment were put together into the device configuration of FTO/CdS/$Sb_2(SSe)_3$/DEA(Cl)/Spiro-OMeTAD/Au. The respective cross-sectional SEM micrograph (Figure 3a) has indicated the device whole structure with apparent multiple layers. The corresponding J-V curves for the control and modified $Sb_2(SSe)_3$ based devices are plotted in Figure 3b, whereas, the parameters of the device are listed inset. We have also checked the other concentration of DEA(Cl) (0 to 3 $mgmL^{-1}$) (Figure S5) and find out the 2 $mgmL^{-1}$ was an optimized ratio and employed it for further experimentation. The control device without DEA(Cl)-modification delivers a PCE of 7.14%, with V_{OC}, a short-circuit current density (J_{SC}), and a FF of 0.59 V, 22.86 mA cm^{-2}, and 54.9%, respectively. To improve the film quality, we spin-coated DEA(Cl) solution on $Sb_2(SSe)_3$ film with optimized concentration in IPA. The Champion device performance was thus improved to 9.17%, and the corresponding V_{OC}, J_{SC}, and FF are 0.63 V, 24.69 mA cm^{-2}, and 59%, respectively. An apparent improvement in V_{OC} was observed from 0.55 to 0.63 V for the modified devices. This improvment in V_{OC} can be assigned to the surface treatment strategy of the DEA(Cl)-modifier, due to the improvement in crystallinity and enhanced grain size of $Sb_2(SSe)_3$ film (Figure 2). The increment in V_{OC} could be attributed to the reduced recombination, which will be explained in detail with further electrical characterizations. Furthermore, the reason behind the increment in J_{SC} and FF from 20 to 24 $mAcm^{-2}$ and 56 to 62%, respectively, for the modified devices can be attributed to the improvement in conductivity of $Sb_2(SSe)_3$ film (Figure 2f). Furthermore, the modified device presents negligible efficiency hysteresis as compared to its counterpart (Figure S6, Table S1). Additionally, the durability of as-fabricated devices was explored with devices aged in the inert

environment with humid conditions of 30 to 40% at room temperature. DEA(Cl)-based devices present better stability than the control devices (Figure S7a-b, supporting information). Specifically, the DEA(Cl)-based device was kept more than 91% of the initial efficiency after aging for 30 days (Figure S7a), whereas the efficiency of control device decreases comparatively fast to 72% of its initial value under a similar aging condition (Figure S7b). The corresponding device stability under high humid conditions is proved by our water contact angle measurements control and modified-$Sb_2(SSe)_3$ films (Figure S8). The corresponding results indicate that the DEA(Cl) modifier does not permit the transition of oxygen or water molecules into the surface of $Sb_2(SSe)_3$ film. We suppose that then respective interactivity between DEA(Cl) and $Sb_2(SSe)_3$ enhanced the heterojunction characteristics and solar cells' durability. The external quantum efficiency (EQE) results of the pristine $Sb_2(SSe)_3$ film and DEA(Cl) modified film-based devices are presented in Figure 3c. In comparison to the control device, the DEA(Cl)-based device indicated improved EQE within the range of 300 to 900 nm of wavelength, presenting persuasive carriers separation and accumulation at the interfaces and exceptional quality of the active layer.[37] The integrated J_{SC} for the control and DEA(Cl)-modified devices were calculated to be 18.71 and 22.10 mA cm^{-2}, respectively. The integrated J_{SC} is nearly consistent with the J_{SC} acquired from the J-V curve, however, slightly smaller than that value obtained from the J-V measurements. The corresponding decreased value of J_{SC} could be assigned to the fact the long measurement time, which results in degradation of devices under long-term illumination during EQE measurements diminish the current density.[38] The statistics of PCE for a set of 20 devices are given in Figure 3d, and it is impressive to observe that the DEA(Cl)-based devices indicate sustainable and improved performance than that of the pristine devices. Additionally, the PCEs of the control devices display wide distribution around 6.6%, whereas, the DEA(Cl) modified devices show a relatively narrower distribution centered at 8.1%. To check the device reproductivity, we have fabricated a set of 20 devices with and without DEA(Cl)-modification, and the corresponding variation in devices parameters is given

in Figure 4a-c. All the fabricated solar cells were measured under the same measuring conditions with an active device area of 0.09 cm^2. It can be observed that, in comparison to the control devices, solar cells modified with DEA(Cl) show improved overall performance with the aid of all device parameters.

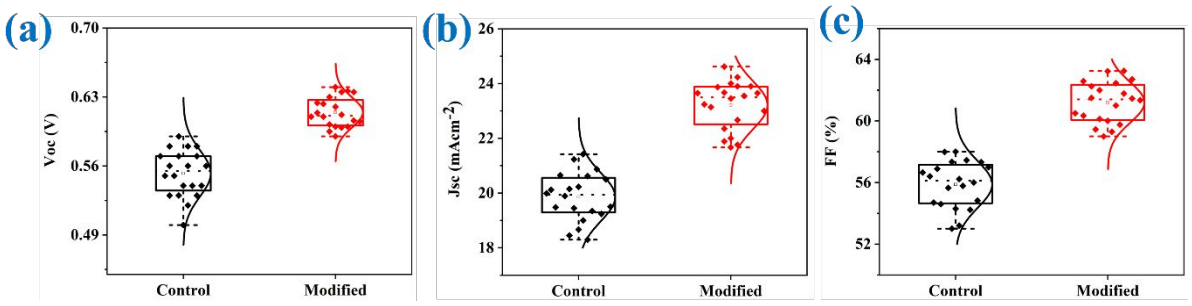

Figure 4. Statistical analysis device parameters (a) V_{OC} (b) J_{SC} (c) FF comparison of control and modified devices.

To further examine the enhanced performance of the DEA(Cl)-modified device systematically, dark J-V measurements were carried out for both pristine $Sb_2(SSe)_3$ and $Sb_2(SSe)_3$/DEA(Cl) samples. Figure 5a shows the dark J-V curves of the corresponding devices. The modified device shows excellent rectification characteristics as compared to the control device, which indicates that DEA(Cl) was successfully suppressed the leakage current density. Furthermore, the impact of DEA(Cl) modification on the boosted performance is also studied via junction quality measurements of pure $Sb_2(SSe)_3$ and $Sb_2(S,Se)_3$/DEA(Cl)-based devices. Here, we have employed Site's mechanism (equation 1) to calculate junction quantities, such as, reverse saturation current density (J_o), ideality factor of the diode (A), shunt conductance (G), and series resistance (R_s) with and without DEA(Cl)-modified devices.[39]

$$J = J_o \exp\left[\frac{q}{AKT}(V - JR)\right] + GV - J_L \quad (1)$$

The shunt conductance G were calculated as 4.4 and 0.27 $mScm^{-2}$ for the pristine- $Sb_2(SSe)_3$ and $Sb_2(SSe)_3$/DEA(Cl) devices, respectively, by deriving from the flat regions of the plots of dJ/dV over V under, as shown in Figure 5b. The series resistance (R_s) was extracted from the plots of dV/dJ over $(J + J_{SC})^{-1}$ extending to the Y-axis, whereas the ideality factor (A) was

obtained from the slope of AkT/q (Figure 5c). The values of sheet resistance were calculated to be 1.20 and 0.76 Ω cm^2 for the control and DEA(Cl)-modified devices, respectively, whereas, the values of ideality factor were 4.2 and 1.95 for the corresponding devices. The reduced values of R_s and A for DEA(Cl)-treated device in comparison to the control device, suggesting suppressed interfacial recombination losses. In the end, the reverse saturation current J_o was obtained from the J + J_{SC} - GV over V-RJ plot (Figure 4d). The values of J_o were extracted to be 5.5 x 10^{-2} and 6.1 x 10^{-3} $mAcm^{-2}$ from the intercept of the curve of the control and DEA(Cl)-modified devices, respectively. Consequently, the obtained results indicated that the surface modifier DEA(Cl) could remarkably improve the $Sb_2(SSe)_3$/HTL heterojunction characteristics, as concluded from the efficiently-suppressed values of J_o and A for the DEA(Cl)-based device. Moreover, the corresponding modification has also decreased the charge transfer resistance and therefore, improved the device parameters in terms of V_{OC} and FF of the device. Additionally, the defect states passivation effect of DEA(Cl) was explored using a single device structure and calculated by employing the space charge limited current method.[40] Figure 5e and f represent the dark J-V curves of the control and $Sb_2(S,Se)_3$/DEA(Cl) devices, respectively. Commonly, the respective J-V graph of control and modified devices can be categorized into three regions depending on the values of exponent (n): when the value of n is one (at smaller voltage), the region is known as the Ohmic region, the region at a middle voltage (n > 3) is assigned to the trap-filled limit (TFL) region and the third region at large voltage (n = 2) is known as Child region. In the TFL domain, the current quickly enhances when the bias voltage surpasses the wrinkle point, suggesting that the ionic defects are entirely occupied by the infused carriers. The trap-filled limited voltages (V_{TFL}) for the control and DEA(Cl)-modified devices were extracted as 0.46 and 0.24 V, respectively, and the trap state density n_{trap} of corresponding devices can be determined by the given equation,[40] as in Eq. (2):

$$n_{trap} = \frac{2\varepsilon\varepsilon_o V_{TFL}}{qL^2} \quad (2)$$

where ε vacuum permittivity, ε_o relative permittivity whose value is calculated to be 15 for $Sb_2(SSe)_3$ in literature,[22] q is the charge carrier in the film, and L is the thickness of $Sb_2(SSe)_3$ film. Interestingly, the modified device presented a much lower value of trap states density (3.8 x 10^{15} cm^{-3}) in comparison to the control device (7.4 x 10^{15} cm^{-3}) (Table S2), which could be assigned to its exceptional quality of $Sb_2(SSe)_3$ active layer with the DEA(Cl) treatment, as evidenced by the XRD and SEM results. Furthermore, the improvement in V_{OC} by the DEA(Cl) modification of $Sb_2(SSe)_3$ thin film is further confirmed by capacitance-voltage (C–V) measurement, which is the common technique to obtain the V_{bi} as given by the following equation:

$$\frac{1}{C^2} = \frac{2}{q\varepsilon_s N_A}\left(V_{bi} - V - \frac{2kT}{q}\right) \quad (3)$$

Figure 5g presents the $1/C^2$–V curves and the value of V_{bi} is extracted from the linear fitting of graph extrapolating to x-axis. The corresponding values of V_{bi} of the of control and modified devises can be determined as 0.72 and 0.87 V, respectively. This implying that the improved V_{bi} of modified device indicated that the DEA(Cl) modification remarkably enhanced the quality $Sb_2(SSe)_3$/HTL heterojunction interface, which is consistent with the above electrical analysis results. It can be concluded that immense increase in the V_{OC} of the treated device corresponds to the enhancement in built-in electric field.[14] To interrogate the interfacial charge transport characteristics of the fabricated solar cells, we execute electrical impedance spectroscopy (EIS) analysis. Figure 5h indicates the Nyquist plots of the devices with and without DEA(Cl) modification, whereas the inset shows the corresponding circuit model of the measurements. The x-axis cut-off is ascribed to series resistance R_S, which corresponds to the active layer resistance and the interfacial resistance of the corresponding interfaces, whereas the arc size is indicating the recombination resistance (R_{rec}), which is inversely related to the non-radiative recombination of charges at the interfaces.[41] It can be seen that the R_S of the control device is larger than that of the treated device, and the reverse trend is obtained for R_{rec},

which is due to the decline in $Sb_2(SSe)_3$ defect density for the modified device. This remarkably suppressed recombination process is one factor bring about V_{OC} improvement. The purpose of modification with DEA(Cl) of $Sb_2(SSe)_3$ film was not only to improve the crystal quality and morphology but also to modify its energy levels to promote the photogenerated charge carriers transfer across the corresponding hole and electron transport layer in a solar cell.

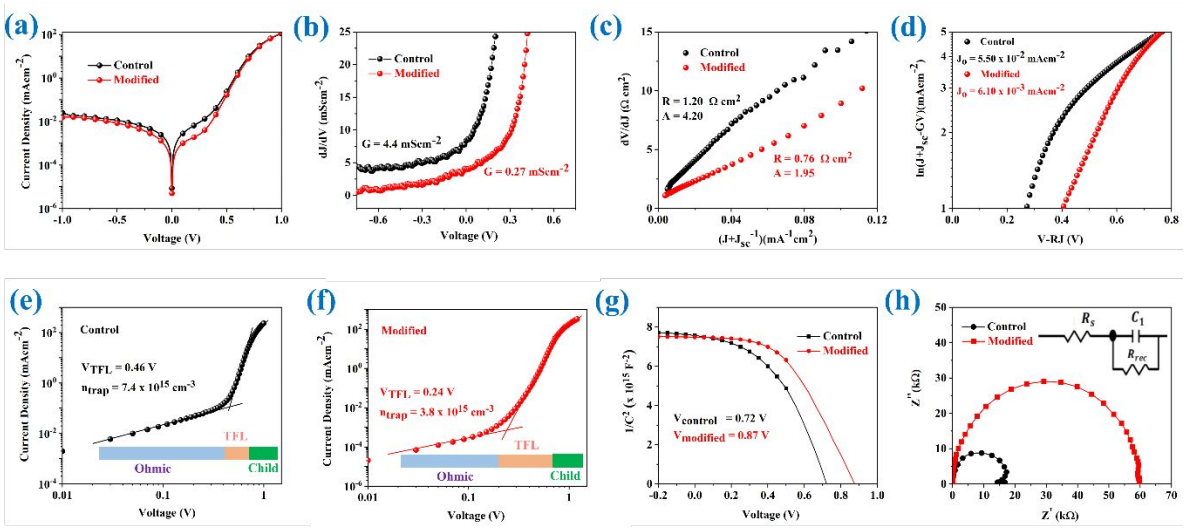

Figure 5. Electrical behaviours of the corresponding control and modified devices: (a) J-V characteristics under dark conditions (b) dJ/dV vs V curves of control and modified devices, (c) dJ/dV vs $(J+J_{SC})^{-1}$ curves of corresponding devices, (d) reverse saturation current density Jo characterizations, (e) and (f) are dark J-V spectra of the control and modified devices, respectively, (device structure, FTO/CdS/$Sb_2(SSe)_3$/with and without DEA(Cl)/Au). (g) $1/C^2$ versus V graph to evaluate V_{bi} (h) Nyquist plots for the corresponding devices without and with DEA(Cl) modification.

Ultraviolet photoelectron spectroscopy (UPS) was employed to evaluate conduction bands (E_C), valance bands (E_V), and Fermi levels (E_f), to further explore the impact of DEA(Cl)-modification on the energy levels of $Sb_2(SSe)_3$. As a result, the E_C, E_V and E_f of control $Sb_2(SSe)_3$ film were calculated as -3.90, -5.42 and -4.57 eV, respectively, according to the bandgap obtained from the Tauc plot (Figure S9). On the other hand, the respective E_C, E_V and

E_f of the modified film were obtained as -3.80, -5.32, and -4.12 eV, respectively (Figure 6a, b). The E_f of DEA(Cl)-treated film was upshifted compared to the control film, suggesting that the conductivity of $Sb_2(SSe)_3$ film is increased (Figure 2f) and lead to the enhancement in carrier density with the aid of DEA(Cl), which is also prove by C–V measurement.[42] The upshift of E_f is responsible for the improvement in V_{OC}.[43] Figure 6c indicates the complete energy levels of the whole device with various active layers of control and modified $Sb_2(SSe)_3$ film. The respective CBM and VBM for HTL and ETL were extracted from the reported work.[7] It was observed that the conduction band level of pristine $Sb_2(SSe)_3$ film is beneath the conduction band level of CdS (-3.83 eV), which creates the energy barrier for electron transfer. Whereas, the conduction band level of modified $Sb_2(SSe)_3$ film upshifts slightly, thus generating a closely-matched conduction band level with the corresponding ETL level. This promotes the diffusion of photogenerated electrons across the interface of CdS/$Sb_2(SSe)_3$ and suppresses the energy consumption of electrons. For the hole carriers collection by the HTL, the valance band level position of the control film is lower than that of valance band level of hole transport layer (-5.20 eV). The optimized device acquires a valance band level that is closer to that of HTL and this permits the DEA(Cl)-modified device to transport holes with efficiently suppressed energy loss. The favorable energy level matching (with DEA(Cl)-modification) of the complete device represents the effective withdrawal of charge carriers without producing unnecessary non-radiative recombination, therefore, promoting the charge transport to the respective transfer films, and leading to an improved J_{SC}.

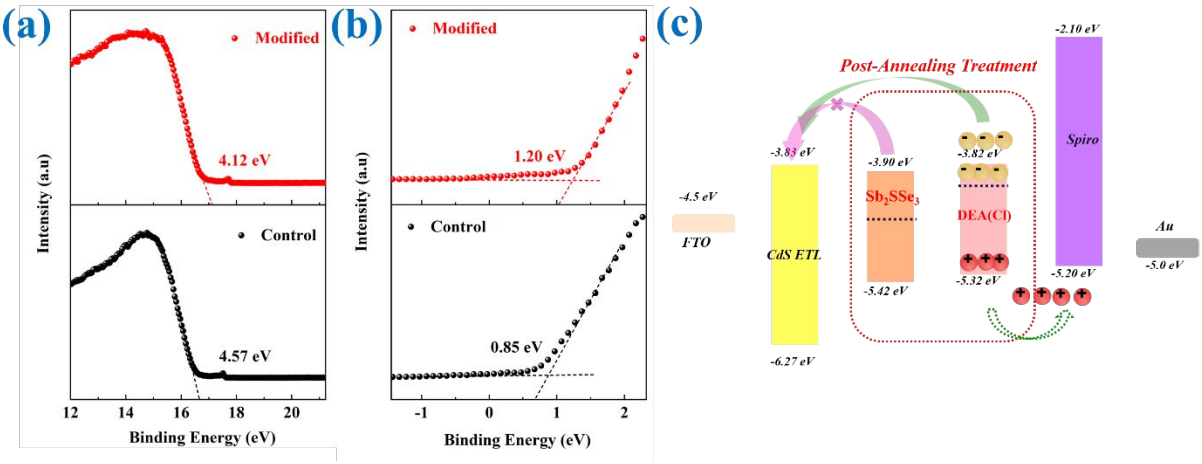

Figure 6. (a) Valance band position (b) Second electron cut-off region of $Sb_2(SSe)_3$ films with and without modification by UPS measurements. (c) A band alignment diagram of $Sb_2(SSe)_3$ devices with and without DEA(Cl) treatment.

3. Conclusions

In summary, organic chloride salt (DEA(Cl)) has been introduced into IPA-based precursor solutions for the first time and demonstrated a successful process of modification of $Sb_2(SSe)_3$ film fabricated through the hydrothermal method. The corresponding modification of $Sb_2(SSe)_3$ film not only improved the crystallinity and morphology but also successfully suppressed the impurities (Sb_2O_3) in the film. As a result, reduced defects states, high built-in potential, and preferred energy band alignment for the whole device were promptly acquired. Consequently, the optimized modification of $Sb_2(SSe)_3$ based device presents an improved performance from 7.41% to 9.17%. This research suggests that the DEA(Cl)-modification of $Sb_2(SSe)_3$ film is a promising strategy for the development of high-performance Sb-based photovoltaic.

4. Experimental details

Cadmium sulfide (CdS) electron transport layer was fabricated onto the FTO glasses, cleaned with soap, DI water, ethanol and isopropyl alcohol (IPA) under sonication each for 20 mints, using chemical bath deposition (CBD) by following our previous research.[23] Afterwards, the

samples were quickly washed via DI water and ethanol, respectively, and put into the oven for 30 min. Finally, we have spin-coated $CdCl_2$/methanol solution on the corresponding CdS films and then annealed sequentially at 100 and 400 C˚, respectively, for 6 min each.

We have employed a standard hydrothermal method to fabricate the $Sb_2(SSe)_3$ film onto CdS layer. The raw materials $C_4H_4KO_7Sb{\cdot}0.5H_2O$ (20 mM), $Na_2S_2O_3{\cdot}5H_2O$ (80 mM), and selenourea (CH_4N_2Se) (4.5 mM) were applied as Sb, S, and Se source, respectively, and dissolved into 40 mL DI water under stirring until obtained light yellow semi-transparent solution in the inner Teflon tank of autoclave (50 mL). Then FTO/CdS samples were immersed into the prepared solution and tilted with an angle of 75°. Then the autoclave was sealed and placed into an oven at 140 °C for 2 hours and 20 min to start the development of $Sb_2(SSe)_3$ film with a suitable thickness. The acquired $Sb_2(SSe)_3$ films were subsequently rinsed with DI water and ethanol to remove the residual on the film surface by following the reported method.[7] Finally, to remove the samples from the glass strip, the samples were put into the vacuum oven at 110 °C for one min, and then transferred to the N_2-glove box for annealing at 350 °C for 10 min. For DEA(Cl)-modification of $Sb_2(SSe)_3$ film, we have prepared the DEA(Cl) precursor solution in IPA and then deposited on the $Sb_2(SSe)_3$ samples via spin-coating method (3000rmp/30s) and annealed at optimized temperature (100˚C) for 10 min under N_2-environment. For HTL, first, we have prepared the corresponding solution by dissolving 36.6 mg mL^{-1} of Spiro-OMeTAD powder into the chlorobenzene and then 14.5 and 9.5 µL of 4-tert-butylpyridine (tBP) lithium bis(trifluoromethanesulfonyl)imide (LiTFSI) solution were sequentially added into spiro-OMeTAD solution. The corresponding prepared solution was deposited onto the $Sb_2(SSe)_3$/DEA(Cl) surface at 4000 rpm for 30 s, and then annealed at 105°C for 10 min under inert environment. Finally, the Au counter electrode was fumed to complete the device by employing thermal evaporator. The device performance of the devices was measured under solar illumination of intensity 100 mW/cm^2 AM 1.5 G using a class AAA solar simulator.

$Sb_2(SSe)_3$ films morphology and cross-sectional micrographs of the whole device were acquired from SEM, SUPRA 55. XRD, Ultima-iv, with working parameters of 40 kV and 40 mA, was employed to get XRD measurements of $Sb_2(SSe)_3$ films. The EQE spectra of devices were measured via Keithley 2400 and Zolix SCS101 system. EDS, BRUKER QUANTAX 200 was used to get the EDX analysis of the corresponding $Sb_2(SSe)_3$ films. The C-V results of the whole devices were measured via Keithley source meter using measuring parameters of (AC amplitude of 30 mV, frequency of 10 kHz). A contact angle meter (PERFECT WAM-100) was employed to obtain the water contact angles results.

ASSOCIATED CONTENT

Supporting Information

The Supporting Information is available free of charge on the ACS Publications website at DOI: Magnified SEM images, Hysteresis measurements, absorbance spectra, device stability data, XPS data, water contact angle results, photovoltaic data, PL spectra, and supporting tables

Notes

The authors declare no competing financial interest.

AUTHOR INFORMATION

Corresponding Author Email: lgx@szu.edu.cn

ACKNOWLEDGMENT

This work was supported by National Natural Science Foundation of China (62074102, 62104157 and 62104156, China), Key Project of Department of Education of Guangdong Province (2018KZDXM059, China), Science and Technology plan project of Shenzhen

(JCYJ20190808153409238 and 20200812000347001, China) and Natural Science Foundation of Guangdong Province (2020A1515010805, China).

REFERENCES

1. Green, M. A.; Dunlop, E. D.; Hohl-Ebinger, J.; Yoshita M.; Kopidakis, N.; Hao, X. J.; Solar Cell Efficiency Tables (version 58). *Prog. Photovolt.: Res. Appl.* **2021,** *29* (7), 657-667.

2. Kondrotas, R.; Chen, C.; Tang, J., Sb_2S_3 Solar Cells. *Joule* **2018,** *2* (5), 857-878.

3. Chen, S.; Liu, T.; Zheng, Z.; Ishaq, M.; Liang, G.; Fan, P.; Chen, T.; Tang, J., Recent Progress and Perspectives on Sb_2Se_3-based Photocathodes for Solar Hydrogen Production via Photoelectrochemical Water Splitting. *J. Energy Chem*. **2021**, *67*, 508-523.

4. Li, Z.; Liang, X.; Li, G.; Liu, H.; Zhang, H.; Guo, J.; Chen, J.; Shen, K.; San, X.; Yu, W.; Schropp, R. E. I.; Mai, Y., 9.2%-Efficient Core-Shell Structured Antimony Selenide Nanorod Array Solar Cells. *Nat. Comm.* **2019,** *10* (1), 125.

5. Wang, L.; Li, D.B.; Li, K.; Chen, C.; Deng, H.X.; Gao, L.; Zhao, Y.; Jiang, F.; Li, L.; Huang, F.; He, Y.; Song, H.; Niu, G.; Tang, J., Stable 6%-Efficient Sb_2Se_3 Solar Cells with a Zno Buffer Layer. *Nat. Energy* **2017,** *2* (4), 17046.

6. Tang, R.; Wang, X.; Jiang, C.; Li, S.; Liu, W.; Ju, H.; Yang, S.; Zhu, C.; Chen, T., n-Type Doping of Sb_2S_3 Light-Harvesting Films Enabling High-Efficiency Planar Heterojunction Solar Cells. *ACS Appl. Mater. Interfaces* **2018,** *10* (36), 30314-30321.

7. Tang, R.; Wang, X.; Lian, W.; Huang, J.; Wei, Q.; Huang, M.; Yin, Y.; Jiang, C.; Yang, S.; Xing, G.; Chen, S.; Zhu, C.; Hao, X.; Green, M. A.; Chen, T., Hydrothermal Deposition of Antimony Selenosulfide Thin Films Enables Solar Cells with 10% Efficiency. *Nat. Energy* **2020,** *5* (8), 587-595.

8. Liu, T.; Liang, X.; Liu, Y.; Li, X.; Wang, S.; Mai, Y.; Li, Z., Conduction Band Energy-Level Engineering for Improving Open-Circuit Voltage in Antimony Selenide Nanorod Array Solar Cells. *Adv. Sci.* **2021,** *8* (16), e2100868.

9. Tang, R.; Zheng, Z.H.; Su, Z.H.; Li, X.J.; Wei, Y.D.; Zhang, X.H.; Fu, Y.Q.; Luo, J.T.; Fan, P.; Liang, G.X., Highly Efficient And Stable Planar Heterojunction Solar Cell Based on Sputtered and Post-Selenized Sb_2Se_3 Thin Film. *Nano Energy* **2019,** *64*, 103929.

10. Liang, G.X.; Zheng, Z.H.; Fan, P.; Luo, J.T.; Hu, J.G.; Zhang, X.H.; Ma, H.L.; Fan, B.; Luo, Z.K.; Zhang, D.P., Thermally Induced Structural Evolution and Performance of Sb_2Se_3 Films and Nanorods Prepared By an Easy Sputtering Method. *Sol. Energy Mater. Sol. Cells* **2018,** *174*, 263-270.

11. Shockley, W.; Queisser, H. J., Detailed Balance Limit of Efficiency of p-n Junction Solar Cells. *J. Appl. Phy.* **1961,** *32* (3), 510-519.

12. Lei, H.; Chen, J.; Tan, Z.; Fang, G., Review of Recent Progress in Antimony Chalcogenide-Based Solar Cells: Materials and Devices. *Sol. RRL* **2019,** *3* (6), 1900026.

13. El-Sayad, E. A., Compositional Dependence of the Optical Properties of Amorphous $Sb_2Se_{3-X}S_x$ Thin Films. *J. Non-Cryst. Solids* **2008,** *354* (32), 3806-3811.

14. Shen, K.; Zhang, Y.; Wang, X.; Ou, C.; Guo, F.; Zhu, H.; Liu, C.; Gao, Y.; Schropp, R. E. I.; Li, Z.; Liu, X.; Mai, Y., Efficient and Stable Planar n-i-p Sb_2Se_3 Solar Cells Enabled by Oriented 1D Trigonal Selenium Structures. *Adv. Sci.* **2020,** *7* (16), 2001013.

15. Liang, G.X.; Luo, Y.D.; Chen, S.; Tang, R.; Zheng, Z.H.; Li, X.J.; Liu, X.S.; Liu, Y.K.; Li, Y.F.; Chen, X.Y.; Su, Z.H.; Zhang, X.H.; Ma, H.L.; Fan, P., Sputtered and Selenized Sb_2Se_3 Thin-Film Solar Cells with Open-Circuit Voltage Exceeding 500 Mv. *Nano Energy* **2020,** *73*, 104806.

16. Jaramillo Quintero, O. A.; Rincón, M. E.; Vásquez García, G.; Nair, P. K., Influence of the Electron Buffer Layer on the Photovoltaic Performance of Planar $Sb_2(S_xSe_{1-X})_3$ Solar Cells. *Prog. Photovolt.: Res. Appl.* **2018,** *26* (9), 709-717.

17. Choi, Y. C.; Lee, Y. H.; Im, S. H.; Noh, J. H.; Mandal, T. N.; Yang, W. S.; Seok, S. I., Efficient Inorganic-Organic Heterojunction Solar Cells Employing $Sb_2(S_x/Se_{1-x})_3$ Graded-Composition Sensitizers. *Adv. Energy Mater.* **2014,** *4* (7), 1301680.

18. Wu, C.; Lian, W.; Zhang, L.; Ding, H.; Jiang, C.; Ma, Y.; Han, W.; Li, Y.; Zhu, J.; Chen, T.; Zhu, C., Water Additive Enhanced Solution Processing of Alloy $Sb_2(S_{1-x}Se_x)_3$-Based Solar Cells. *Sol. RRL* **2020,** *4* (5), 1900582.

19. Wu, C.; Zhang, L.; Ding, H.; Ju, H.; Jin, X.; Wang, X.; Zhu, C.; Chen, T., Direct Solution Deposition of Device Quality $Sb_2S_{3-X}Se_x$ Films for High Efficiency Solar Cells. *Sol. Energy Mater. Sol. Cells* **2018,** *183*, 52-58.

20. Wu, C.; Jiang, C.; Wang, X.; Ding, H.; Ju, H.; Zhang, L.; Chen, T.; Zhu, C., Interfacial Engineering by Indium-Doped CdS for High Efficiency Solution Processed $Sb_2(S_{1-x}Se_x)_3$ Solar Cells. *ACS Appl. Mater. Interfaces* **2019,** *11* (3), 3207-3213.

21. Zhang, Y.; Li, J.; Jiang, G.; Liu, W.; Yang, S.; Zhu, C.; Chen, T., Selenium-Graded $Sb_2(S_{1-x}Se_x)_3$ for Planar Heterojunction Solar Cell Delivering a Certified Power Conversion Efficiency of 5.71%. *Sol. RRL* **2017,** *1* (5), 1700017.

22. Wang, W.; Wang, X.; Chen, G.; Yao, L.; Huang, X.; Chen, T.; Zhu, C.; Chen, S.; Huang, Z.; Zhang, Y., Over 6% Certified $Sb_2(S,Se)_3$ Solar Cells Fabricated via In Situ Hydrothermal Growth and Postselenization. *Adv. Electr. Materi.* **2019,** *5* (2), 1800683.

23. Luo, Y.D.; Tang, R.; Chen, S.; Hu, J.G.; Liu, Y.K.; Li, Y.F.; Liu, X.S.; Zheng, Z.H.; Su, Z.H.; Ma, X.F.; Fan, P.; Zhang, X.H.; Ma, H.L.; Chen, Z.G.; Liang, G.X., An Effective Combination Reaction Involved with Sputtered and Selenized Sb Precursors for Efficient Sb_2Se_3 Thin Film Solar Cells. *Chem. Eng. J.* **2020,** *393*, 124599.

24. Wen, X.; Chen, C.; Lu, S.; Li, K.; Kondrotas, R.; Zhao, Y.; Chen, W.; Gao, L.; Wang, C.; Zhang, J.; Niu, G.; Tang, J., Vapor Transport Deposition of Antimony Selenide Thin Film Solar Cells With 7.6% Efficiency. *Nat. Comm.* **2018,** *9* (1), 2179.

25. Yang, B.; Qin, S.; Xue, D.-j.; Chen, C.; He, Y.S.; Niu, D.; Huang, H.; Tang, J., In Situ Sulfurization to Generate $Sb_2(Se_{1-x}S_x)_3$ Alloyed Films and Their Application for Photovoltaics. *Prog. Photovolt.: Res. Appl.* **2017,** *25* (1), 113-122.

26. Ishaq, M.; Chen, S.; Farooq, U.; Azam, M.; Deng, H.; Su, Z.H.; Zheng, Z.H.; Fan, P.; Song, H.S.; Liang, G.X., High Open-Circuit Voltage in Full-Inorganic Sb_2S_3 Solar Cell via Modified Zn-Doped TiO_2 Electron Transport Layer. *Sol. RRL* **2020,** *4* (12), 2000551.

27. Li, K.; Wang, S.; Chen, C.; Kondrotas, R.; Hu, M.; Lu, S.; Wang, C.; Chen, W.; Tang, J., 7.5% n–i–p Sb_2Se_3 Solar Cells with CuSCN as a Hole-Transport Layer. *J. Mater. Chem. A* **2019,** *7* (16), 9665-9672.

28. Chen, C.; Li, K.; Chen, S.; Wang, L.; Lu, S.; Liu, Y.; Li, D.; Song, H.; Tang, J., Efficiency Improvement of Sb_2Se_3 Solar Cells via Grain Boundary Inversion. *ACS Energy Lett.* **2018,** *3* (10), 2335-2341.

29. Choi, Y. C.; Seok, S. I., Efficient Sb_2S_3-Sensitized Solar Cells Via Single-Step Deposition of Sb_2S_3 Using S/Sb-Ratio-Controlled $SbCl_3$-Thiourea Complex Solution. *Adv. Funct. Mater.* **2015,** *25* (19), 2892-2898.

30. Azam, M.; Khan, A. A.; Liang, G.X.; Li, G.J.; Chen, S.; Zheng, Z.H.; Farooq, U.; Ishaq, M.; Fan, P.; Wang, Z.; Wang, Z.G., Examining the Interfacial Defect Passivation with Chlorinated Organic Salt for Highly Efficient and Stable Perovskite Solar Cells. *Sol. RRL* **2020,** *4* (11), 2000358.

31. Oku, T.; Ohishi, Y.; Suzuki, A.; Miyazawa, Y., Effects of Cl Addition to Sb-Doped Perovskite-Type $CH_3NH_3PbI_3$ Photovoltaic Devices. *Metals* **2016**, *6* (7), 147.

32. Jiang, C.; Zhou, J.; Tang, R.; Lian, W.; Wang, X.; Lei, X.; Zeng, H.; Zhu, C.; Tang, W.; Chen, T., 9.7%-Efficient $Sb_2(S,Se)_3$ Solar Cells with a Dithieno[3,2-B: 2′,3′-D]Pyrrole-Cored Hole Transporting Material. *Energy Environ. Sci.* **2021,** *14* (1), 359-364.

33. Liu, D.; Tang, R.; Ma, Y.; Jiang, C.; Lian, W.; Li, G.; Han, W.; Zhu, C.; Chen, T., Direct Hydrothermal Deposition of Antimony Triselenide Films for Efficient Planar Heterojunction Solar Cells. *ACS Appl. Mater. Interfaces* **2021,** *13* (16), 18856-18864.

34. Sulas, D. B.; London, A. E.; Huang, L.; Xu, L.; Wu, Z.; Ng, T. N.; Wong, B. M.; Schlenker, C. W.; Azoulay, J. D.; Sfeir, M. Y., Preferential Charge Generation at Aggregate Sites in Narrow Band Gap Infrared Photoresponsive Polymer Semiconductors. *Adv. Opt. Mater.* **2018,** *6* (7), 1701138.

35. Gao, C.; Huang, J.; Li, H.; Sun, K.; Lai, Y.; Jia, M.; Jiang, L.; Liu, F., Fabrication of Sb_2S_3 Thin Films by Sputtering and Post-Annealing for Solar Cells. *Ceram. Int.* **2019,** *45* (3), 3044-3051.

36. Azam, M.; Yue, S.; Xu, R.; Yang, S.; Liu, K.; Huang, Y.; Sun, Y.; Hassan, A.; Ren, K.; Tan, F.; Wang, Z.; Lei, Y.; Qu, S.; Wang, Z., Realization of Moisture-Resistive Perovskite Films for Highly Efficient Solar Cells Using Molecule Incorporation. *ACS Appl. Mater. Interfaces* **2020,** *12* (35), 39063-39073.

37. Liu, F.; Yan, C.; Huang, J.; Sun, K.; Zhou, F.; Stride, J. A.; Green, M. A.; Hao, X., Nanoscale Microstructure and Chemistry of Cu_2ZnSnS_4/CdS Interface in Kesterite Cu_2ZnSnS_4 Solar Cells. *Adv. Energy Mater.* **2016,** *6* (15), 1600706.

38. Saliba, M.; Etgar, L. Current Density Mismatch in Perovskite Solar Cells. *ACS Energy Letters* **2020**, *5* (9), 2886-2888.

39. Sites, J. R.; Mauk, P. H., Diode Quality Factor Determination for Thin-Film Solar Cells. *Sol. Cells* **1989,** *27* (1), 411-417.

40. Azam, M.; Yue, S.; Xu, R.; Liu, K.; Ren, K.; Sun, Y.; Liu, J.; Wang, Z.; Qu, S.; lei, Y.; Wang, Z., Highly Efficient Solar Cells Based on Cl Incorporated tri-Cation Perovskite Materials. *J. Mater. Chem. A* **2018,** *6* (28), 13725-13734.

41. Ma, Y.; Tang, B.; Lian, W.; Wu, C.; Wang, X.; Ju, H.; Zhu, C.; Fan, F.; Chen, T., Efficient Defect Passivation of Sb_2Se_3 Film by Tellurium Doping for High Performance Solar Cells. *J. Mater. Chem. A* **2020,** *8* (14), 6510-6516.

42. Li, Z.; Chen, X.; Zhu, H.; Chen, J.; Guo, Y.; Zhang, C.; Zhang, W.; Niu, X.; Mai, Y., Sb_2Se_3 Thin Film Solar Cells in Substrate Configuration and the Back Contact Selenization. *Sol. Energy Mater. Sol. Cells* **2017,** *161*, 190-196.

43. Elumalai, N. K.; Uddin, A., Open Circuit Voltage of Organic Solar Cells: an In-Depth Review. *Energy Environ. Sci.* **2016,** *9* (2), 391-410.

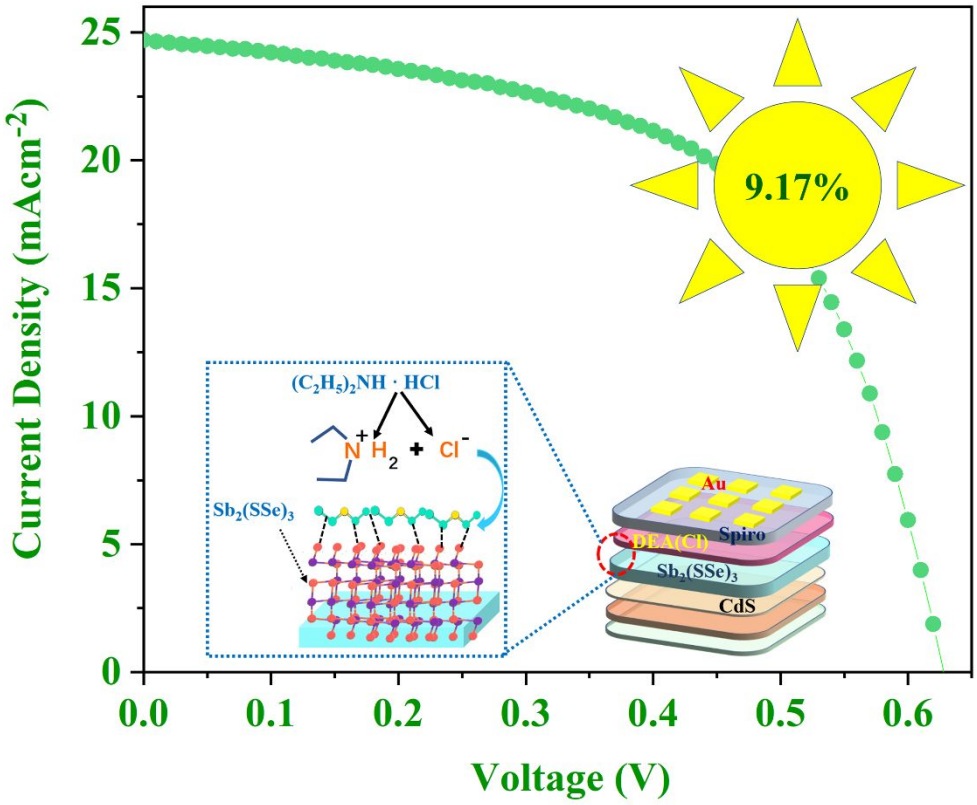

Table of Contents Graphic (TOC)